View Online

GaN grown with InGaN as a weakly bonded layer

Xiaoqing Xu,* Yan Guo, Xianglin Liu,* Jianming Liu, Huaping Song, Biao Zhang, Jun Wang, Shaoyan Yang, Hongyuan Wei, Qinsheng Zhu* and Zhanguo Wang

Received 27th June 2010, Accepted 20th October 2010
DOI: 10.1039/c0ce00345j

GaN thin films were grown with InGaN as an interlayer. The GaN films show different stress states with and without an InGaN interlayer. The influence of the In composition in InGaN on the properties of the high temperature (HT) GaN overlayer was discussed and potential stress-free points were extrapolated. The effect of H_2 on the growth of HT GaN was found to be that it assisted the decomposition of InGaN. A nearly stress free GaN single-crystalline film with mirror-like morphology and single polarity was obtained by inserting an appropriate InGaN interlayer and the growth mechanism of GaN, with a regular network as the template, was discussed. Our research on the controllable growth of high-quality GaN thin film is very important for GaN-based optoelectronic and electronic devices.

Downloaded by Library of Chinese Academy of Sciences on 30 November 2010
Published on 25 November 2010 on http://pubs.rsc.org | doi:10.1039/C0CE00345J

I. Introduction

GaN is a wide gap semiconductor of great promise for application to blue, violet, and ultraviolet (UV) light emitting devices and high temperature (HT) and/or highpower devices.[1,2] One of the critical issues in the development of III–V nitrides for device applications is the lack of a good substrate. Due to the large mismatches of lattice and thermal expansion between GaN and the generally used substrates, such as sapphire, silicon or SiC, high interfacial strain is produced and causes large dislocation densities in the GaN epitaxial layers.[3–6] To release the epilayer strain, compliant substrates have been proposed for lattice-mismatched epitaxy. Improved results for GaN layers grown by metal–organic chemical vapour deposition (MOCVD) on Silicon-on-insulator (SOI) substrates have been reported.[7] Also, the hydrogen-implanted Si substrate has been used for the fabrication of the compliant substrate, and the mismatch strains in the SiC films grown on this substrate have been released and the crystalline qualities have been improved.[8] Recently, self-separated freestanding GaN was obtained using an NH_4Cl interlayer and the NH_4Cl was evaporated during the HT GaN growth, resulting in void formation, which acts as the key for the self-separation of the thick HT GaN.[9]

In this study, we suggest another simple compliant substrate fabrication technique using a combination of InGaN and low temperature (LT) GaN layers to relax the stress in the HT GaN film and the properties of the HT GaN are evaluated. Here, the LT GaN layer provides a template for the HT GaN overlayer. The In atoms in the InGaN layer were evaporated during heating to HT and during the HT GaN growth, resulting in a weakly bonded layer formation, which assists the relaxation of the stress in the overlayer.

Key Laboratory of Semiconductor Materials Science, Institute of Semiconductors, Chinese Academy of Sciences, P.O. Box 912, Beijing 100083, People's Republic of China. E-mail: xxq@semi.ac.cn; xlliu@semi.ac.cn; qszhu@semi.ac.cn

II. Experiments

All the samples in our experiments were grown on (0001) Al_2O_3 substrates in a homemade MOCVD system using NH_3, trimethyl gallium (TMGa) and trimethyl indium (TMIn) as sources. For the growth of sample A, the Al_2O_3 substrate was nitrided with NH_3 gas for 3 min at 1050 °C, prior to the deposition of a 20-nm-thick LT GaN buffer at 550 °C and then a 200-nm-thick GaN film was grown at 1050 °C. The other samples each have an InGaN interlayer inserted between the Al_2O_3 and the LT GaN layer and N_2 diluted TMGa was used to grow the InGaN. The main difference exists in the growth conditions of InGaN. For sample B, the InGaN interlayer was grown at 750 °C and 50 Torr, for sample C it was grown at 580 °C and 300 Torr and for sample D it was grown at 550 °C and 76 Torr. The growth processes of the three InGaN interlayers all last 30 min and the NH_3 was maintained at a constant flow rate of 3 standard litre per minute (SLM).

Field emission scanning electron microscopy (FE-SEM: Sirion and Hitachi S-4800) was used to observe the morphologies of the products. Energy-dispersive X-ray spectroscopy (EDXS) was used to determine the In content in InGaN. X-Ray diffraction (XRD: Rigaku-TTRiii) was used to investigate the epitaxial relationship of the samples. High resolution XRD (HRXRD: Bruker D8 Discover using $CuK_{\alpha 1}$ radiation and the Beijing Synchrotron Radiation Facility) was used to examine the crystallinity and the lattice parameters of the GaN films. The residual stress in the samples was characterized by HR-Raman (JYHR800) scattering using a 514.5 nm line of the argon ion laser. The accuracy during the Raman measurements was 0.3 cm^{-1} with a lateral spatial resolution of 1.0 μm.

III. Results and discussion

A. The growth results

Fig. 1 shows the surface morphologies of the InGaN interlayers (labeled as B_{InGaN}, C_{InGaN}, and D_{InGaN}) of samples B, C, and D. All the three InGaN interlayers show comparatively uniform and integral morphologies and are good soleplates for the

View Online

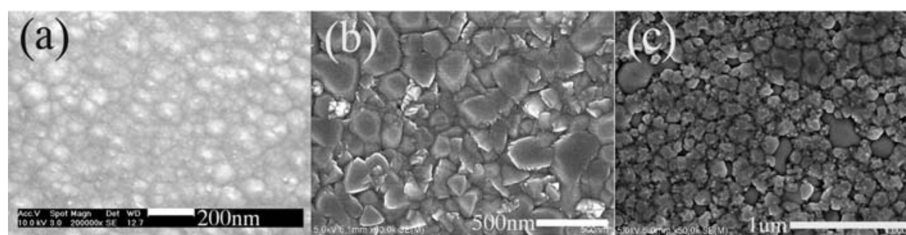

Fig. 1 Surface morphologies of InGaN interlayers (a) B_{InGaN}, (b) C_{InGaN}, (c) D_{InGaN}.

Downloaded by Library of Chinese Academy of Sciences on 30 November 2010
Published on 25 November 2010 on http://pubs.rsc.org | doi:10.1039/C0CE00345J

forthcoming growth of LT GaN and HT GaN. The In compositions are determined by EDXS to be 17.5% for B_{InGaN}, 58.6% for C_{InGaN}, and 80.4% for D_{InGaN}.

Fig. 2 shows the SEM images of the four as-grown GaN samples. Fig. 2(a)–2(d) show the surface morphologies of samples A–D, respectively, and Fig. 2(e)–2(h) show the side views of the corresponding samples. Apparently, samples B and C exhibit smooth and uniform morphologies, while samples A and D have some fluctuations with some pits at the surface. The cross sections of samples B, C, and D exhibit some voids which are produced by the evaporation of In atoms. It is clearly seen that by inserting an appropriate InGaN layer, the surface morphologies of samples B and C are greatly improved.

HR-Raman measurement was carried out to investigate the stress states of the samples, and the Raman spectra of the four GaN samples are shown in Fig. 3. The four samples perform similarly in the Raman spectra, mainly composed of the E_2^H, E_2^L and A_1(LO) modes of GaN, with some peaks originating from the Al_2O_3 substrates as well. Usually, the peak shift of E_2^H is used to represent the stress state and a blueshift is induced by compressive stress, while a redshift is induced by tensile stress.[10] However, the Raman shifts of the E_2^H phonon differ, 566.784 cm^{-1}, 567.803 cm^{-1}, 568.721 cm^{-1} and 568.220 cm^{-1} for samples A, B, C, and D, respectively, indicating different stress states in the four samples. As E_2^H has an intrinsic value of 567.5 cm^{-1} for stress-free GaN,[11] samples B, C and D exhibit compressive stress, while sample A exhibits tensile stress. Of all the four samples, sample B has the minimum stress and is close to the stress-free state.

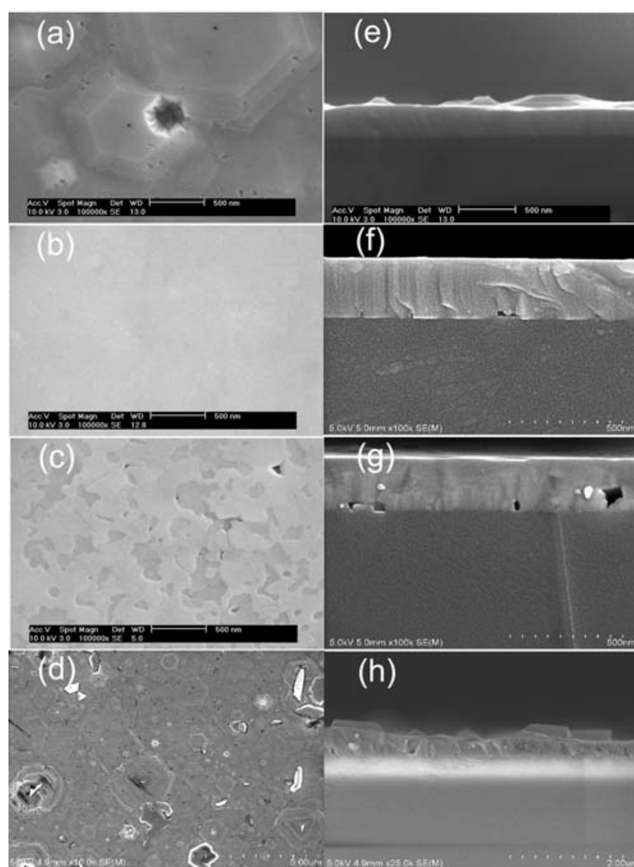

Fig. 2 SEM images of the as-grown samples (a)A, (b)B, (c)C, (d)D by plan view and (e)A, (f)B, (g)C, (h)D by cross-sectional observations.

To further demonstrate the stress states determined from Raman spectra, we also performed HRXRD measurements. The diffraction patterns of the θ–2θ scan of the four samples are shown in Fig. 4. The experimental data are fitted using least-squares refinement with Voigt curve and thus peak positions are precisely determined. The peak positions of GaN (0002) and (0004) are combined to eliminate the zero shift and to evaluate the Bragg angles of GaN (0002)[12] and then the c axis lattice parameters of GaN can be determined. For example, the peak positions of GaN (0002) and (0004) for sample A are 34.6027° and 72.9809°, respectively, so the zero shift is calculated to be −0.0055° and the Bragg angle of GaN (0002) is 17.2959°. Accordingly, the c axis lattice parameters for samples A, B, C and D are determined to be 5.1817 Å, 5.1860 Å, 5.1864 Å and 5.1844 Å, respectively. As the value for the stress-free GaN is 5.185 Å,[9,13] sample A should have a residual tensile stress with samples B and C exhibiting compressive stress, which is consistent with the results obtained from Raman measurement, though sample D exhibits a tiny tensile stress, which is not consistent with the result from Raman measurement. Here, the c axis lattice parameters for samples B and D are close to the stress-free value, though the value for sample D is a little closer. Consequently, the stress states of the samples we have obtained are credible in the main.

All the four GaN samples show c-plane orientation and no signal of InGaN can be observed by XRD. Fig. 5(a) shows the θ–2θ scan of sample B, which is the sample with a tiny stress and best morphology and the θ–2θ scan of B_{InGaN} is also shown for comparison. Both sample B and B_{InGaN} show (0002) and (0004) diffraction peaks and no InGaN peaks can be observed in sample B, indicating no visible In atoms present. Both plan-view and side-view EDXS are measured to further demonstrate the absence of In atoms in sample B, and they are shown in Fig. 5(b) and 5(c). Again no In correlated peaks are observed in Fig. 5(b)

 This journal is © The Royal Society of Chemistry 2010

View Online

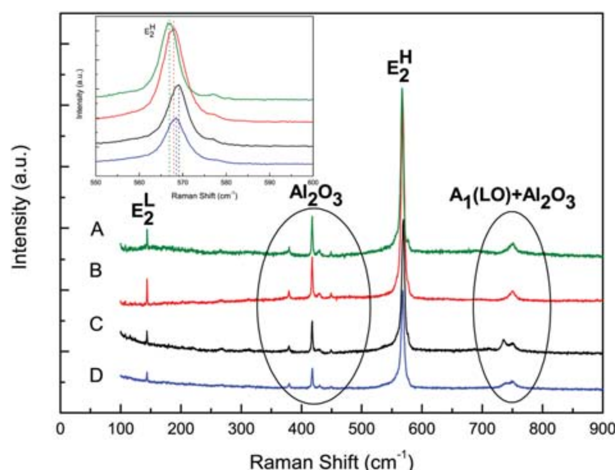

Fig. 3 HR-Raman spectra of the four as-grown samples A, B, C, and D.

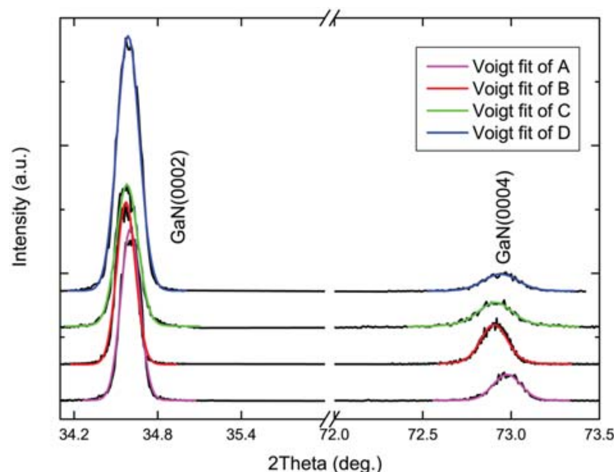

Fig. 4 HRXRD θ–2θ patterns of the four as-grown samples A, B, C, and D.

and 5(c), so we draw the conclusion that no visible In atoms are residual in sample B after the growth of HT GaN.

The smooth and nearly stress free sample B was then etched in hot phosphoric and sulfuric acids (1 : 3 v/v) and the images of the etched sample are shown in Fig. 6(a) and 6(b). Hexagonal pyramids are observed, which indicates N polarity for sample B.[14] This can be explained by the GaN overlayer in sample B inheriting the N polarity from the nitrided sapphire substrate.[15,16]

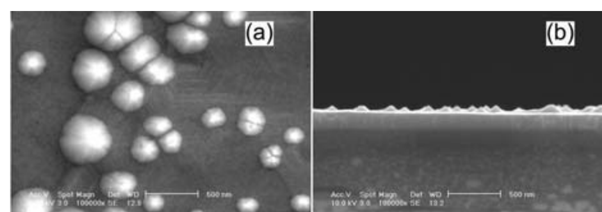

Fig. 6 SEM images of the etched sample B, (a) for the surface and (b) for the cross section.

This leads to an interesting and significant result that the nearly stress free GaN thin film with mirror-like morphology and single polarity can be obtained by inserting an appropriate InGaN interlayer.

B. The influence of In composition in InGaN

To study the influence of In composition in InGaN on the properties of the HT GaN overlayer, we analyzed the decomposition of InGaN theoretically by thermodynamics. As the decomposition rate of InN is about two orders larger than that of GaN,[17] we neglected the decomposition of GaN during heating to HT (1050 °C). Therefore, the decomposition of InGaN can be simply expressed by the reaction:

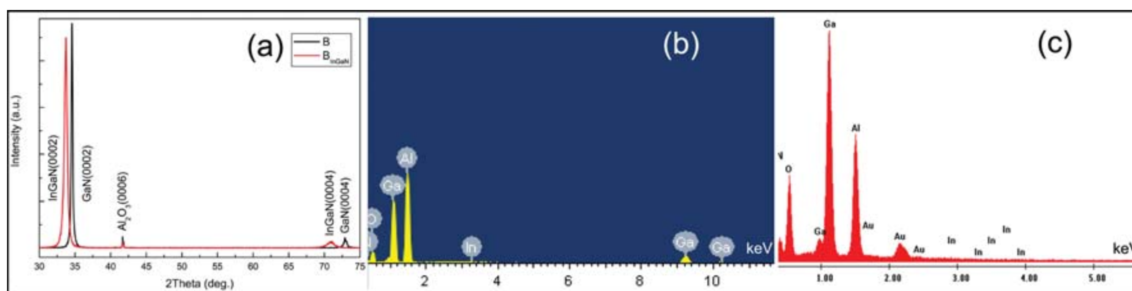

Fig. 5 (a)XRD θ–2θ patterns of sample B and B_{InGaN}, (b) plan-view and (c) side-view EDXS of sample B. Au correlated peaks in (c) come from the gold particles for conductive coating.

Downloaded by Library of Chinese Academy of Sciences on 30 November 2010
Published on 25 November 2010 on http://pubs.rsc.org | doi:10.1039/C0CE00345J

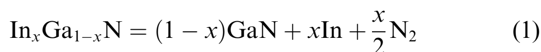

$$In_xGa_{1-x}N = (1 - x)GaN + xIn + \frac{x}{2}N_2 \quad (1)$$

As for the pure InN decomposition reaction, the Gibbs free energy of reaction per mole can be expressed as:

$$\Delta_r G_m = \Delta_r G_m^{\theta} + RTln\left(\frac{P}{P^{\theta}}\right)^{\frac{1}{2}} \quad (2)$$

where $\Delta_r G_m^{\theta}$ is the standard Gibbs free energy of reaction and P, P^{θ} are the partial pressure of N_2 and the standard atmospheric pressure, respectively. When InN decomposition gets to equilibrium, eqn (2) can be modulated to:

$$\Delta_r G_m^0 = \Delta_r G_m^{\theta} + RTln\left(\frac{P^0}{P^{\theta}}\right)^{\frac{1}{2}} = 0 \quad (3)$$

Here, P^0 is the equilibrium partial pressure of N_2. Thereafter, the Gibbs free energy of reaction per mole can be expressed alternatively as:

$$\Delta_r G_m = RTln\frac{\left(\frac{P}{P^{\theta}}\right)^{\frac{1}{2}}}{\left(\frac{P^0}{P^{\theta}}\right)^{\frac{1}{2}}} \quad (4)$$

Finally, as for the InGaN decomposition reaction in eqn (1), the Gibbs free energy of reaction per mole can be elicited:

$$\Delta G_m = x\Delta_r G_m - RT(xlna_I + (1-x)lna_G) \quad (5)$$

where a_I and a_G are the activities of InN and GaN in the InGaN alloy,[18] respectively.

Fig. 7 shows the Gibbs free energies of reaction per mole for $In_xGa_{1-x}N$ decomposition reactions, with $x = 0.175$ to $x = 0.804$. The Gibbs free energies of reaction per mole for the decomposition of pure InN and GaN are marked for comparison. Here, the partial pressure of N_2 is 25 Torr. It is found that for all of the three InGaN interlayers in the temperature range of 550 °C to 1050 °C, $\Delta G_m < 0$ and the higher the In content is, the lower the ΔG_m is. This means that all of the three InGaN interlayers can be decomposed thermodynamically and a higher In content leads to a larger driving force for InGaN decomposition.

To investigate the template before HT GaN growth, we heated the LT GaN/InGaN layers to 1050 °C and then cooled them down. The SEM images of the three annealed templates are shown in Fig. 8. It can be seen in Fig. 8(a) that lots of tiny voids are produced, with a dimension of several nanometres to tens of nanometres, leaving the matrix a continuous network. Fig. 8(b), however, exhibits some big voids with a dimensions from several nanometres to as large as hundreds of nanometres, meaning the network is partly broken off. No network can be found in the annealed template of sample D, and the LT GaN/InGaN layers are almost evaporated, leaving only a small fraction of the layers surrounded by nucleation sites, as shown in Fig. 8(c). This is consistent with the different driving forces for InGaN decomposition with different In contents, as obtained from the thermodynamic calculations. In addition, the more compact microstructure of the InGaN with the lower In composition, than that of the InGaN with high In composition (as is shown in Fig. 1), also contribute to the different decomposition rates of the InGaN interlayers. B_{InGaN}, grown at 750 °C, with the most compact microstructure, should be relatively difficult to decompose, while D_{InGaN}, grown at 550 °C, with the least compact microstructure, should be easier to decompose kinetically. Therefore, the InGaN with a higher In composition is easier to decompose, both thermodynamically and kinetically.

Therewith, we proposed a model to simulate the growth process of GaN, with a regular network as the template and this is sketched in Fig. 9. HT GaN growth was initiated on top of the network and this proceeded to grow laterally over the void region with nearly vertical side-walls. The GaN continued to grow laterally until it coalesced with the laterally growing material from an adjacent mesa. After the film coalescence, the GaN film continued to grow vertically. This is quite similar to the case of lateral epitaxial overgrowth on a patterned substrate[19] and can therefore be considered as self-patterned lateral epitaxial overgrowth.

The Raman shifts of the E_2^H phonon and the c axis lattice parameter shifts of the four GaN samples are plotted as functions of the In content in the InGaN interlayers in Fig. 10. It can be clearly seen that blue shifts of the E_2^H occur as the In content increases and then red shifts take place as the In content further increases. Similarly, the c axis lattice parameter increases as the In content increases and then decreases as the In content further increases. The two sets of data arrive at a uniform trend. There are three types of strains in the GaN/Al_2O_3 heterostructures,[10] tensile strain for lattice misfit, compressive strain for thermal

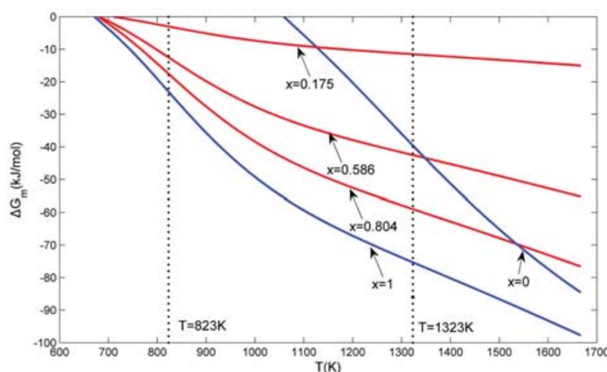

Fig. 7 Gibbs free energies of reaction per mole for $In_xGa_{1-x}N$ decomposition reactions as a function of temperature with different In contents. The partial pressure of N_2 is 25 Torr.

Downloaded by Library of Chinese Academy of Sciences on 30 November 2010
Published on 25 November 2010 on http://pubs.rsc.org | doi:10.1039/C0CE00345J

 This journal is © The Royal Society of Chemistry 2010

View Online

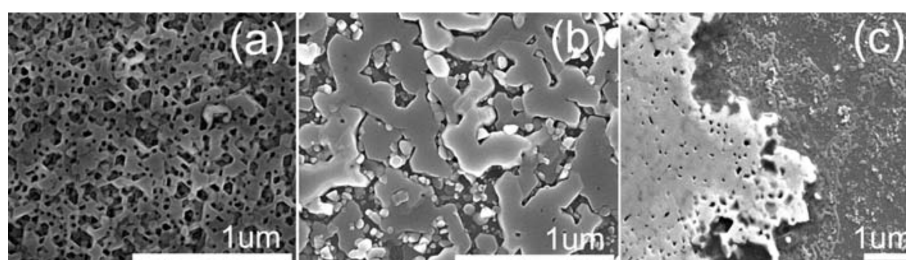

Fig. 8 SEM images of the annealed templates of samples (a) B, (b) C and (c) D.

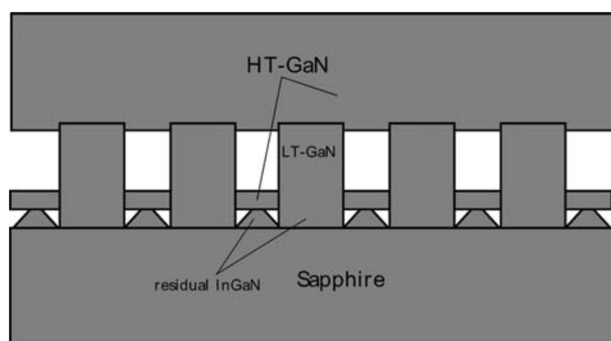

Fig. 9 Growth model of GaN, with a regular network as the template.

Downloaded by Library of Chinese Academy of Sciences on 30 November 2010
Published on 25 November 2010 on http://pubs.rsc.org | doi:10.1039/C0CE00345J

misfit and tensile strain for defect strain. For sample A, there may be residual lattice mismatch strain and defects in it, so it exhibits a visible tensile stress. For samples B and C, the weakly bonded InGaN layers have relieved the lattice mismatch strains and this has resulted in a compressive thermal stress in these samples. Besides, the lesser stress in sample B than in sample C predicates that 17.5 % of In in the InGaN can better relieve the stress. 58.6 % of In may produce voids that are too big in the LT GaN/InGaN template during heating, therefore, the HT GaN overlayer has more contact with the substrate, resulting in a larger compressive thermal stress. Although the stress state of sample D differs in the Raman and HRXRD measurements, the larger *c* axis lattice parameter and larger Raman shift of sample D than those of sample A (without the InGaN interlayer) both indicate the relaxation of the tensile strain. This may be caused by the assistance of a comparatively disordered nucleation layer, as shown in Fig. 8(c), in the relaxation of the lattice mismatch strain. Strain-free points are inferred by extrapolating the two sets of data and two points are obtained from each data set. Two of the four points overlap at around $x = 0.12$ and the other two are at $x = 0.74$ and $x = 0.94$, respectively. However, as discussed above, a high In content leads to a large driving force for InGaN decomposition, leaving no network in the template (like Fig. 8(c)) and leading to a deteriorated morphology (like Fig. 2(d) and 2(h)). Therefore, $x = 0.12$ with a continuous net-like template is the potential point for stress-free GaN growth.

C. The effect of H_2 on the growth of HT GaN

As presented above, a nearly stress-free GaN thin film with mirror-like morphology and single polarity can be obtained by inserting an $In_{0.175}Ga_{0.825}N$ interlayer. However, is it enough just to control the In composition in InGaN? Another sample

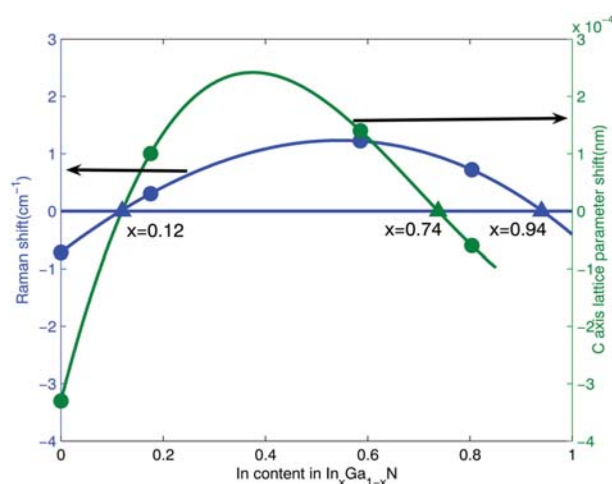

Fig. 10 Raman shifts and *c* axis lattice parameter shifts as functions of the In content in the InGaN interlayers. The round dots are experimental data from Fig. 3 and Fig. 4 and the triangles are extrapolated by the fitting curves to find the stress-free points.

(sample E) was grown in conditions similar to those used for sample B, with the only difference being the carrier gas used during the growth of HT GaN, H_2 was used for sample B and N_2 was used for sample E. Fig. 11 shows the SEM image, XRD rocking curve, Raman spectrum and EDXS of sample E. It is apparent that the surface morphology and the crystallinity of sample E are both worse than those of sample B and a large tensile stress was obtained, as the Raman shift of E_2^H is 565.957 cm^{-1}. What is more, strong fluorescence was observed in the Raman spectrum of sample E. EDXS in Fig. 11(d) exhibits obvious In peaks, indicating the presence of In atoms in sample E. All the poor instances of sample E can be explained by the fact that H_2 can assist in the decomposition of InGaN. N_2 prevents the decomposition of InGaN, based on eqn (1), thus leaving some In atoms in sample E, even after the growth of HT GaN. The In atoms diffuse during the growth of HT GaN and some defects are produced. Therefore, the crystallinity, as well as the morphology of the sample, is deteriorated and the fluorescence in the Raman spectrum is attributed to the defects produced by the diffusion of In atoms. Therefore, the In composition in the interlayer and the H_2 carrier gas used during the growth of HT GaN both play important roles in the controllable growth of high quality GaN thin films.

Through modulation of the In composition in the InGaN interlayer and the flow rate of the H_2 carrier gas, we have

View Online

Downloaded by Library of Chinese Academy of Sciences on 30 November 2010
Published on 25 November 2010 on http://pubs.rsc.org | doi:10.1039/C0CE00345J

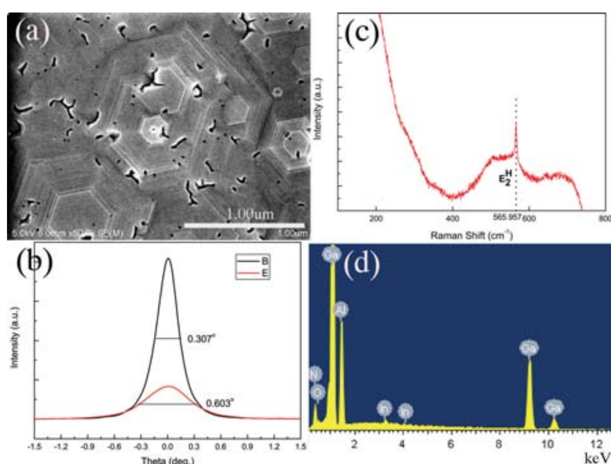

Fig. 11 (a) SEM image, (c) raman spectrum and (d) EDXS of sample E. (b) XRD rocking curves of samples B and E.

obtained a smooth GaN film with a thickness of 200 nm. The GaN (0002) full width at half maximum of the XRD rocking curve is 0.13°. However, more efforts are still needed to further improve the efficiency of the InGaN interlayer.

IV. Conclusions

In summary, a compliant substrate composed of InGaN and LT GaN layers was produced to release the stress in the HT GaN film. The InGaN interlayer with an appropriate In composition can lead to a regular netlike template, for the following growth of GaN, which allows self-patterned lateral epitaxial overgrowth. In this way, a nearly stress-free GaN single-crystalline film with mirror-like morphology and single polarity was obtained. InGaN with 12% of In is a potential interlayer for stress-free GaN growth. H_2 can assist the decomposition of InGaN, while N_2 prevents the decomposition of the InGaN, thus use of a H_2 carrier gas is also crucial for the growth of high quality GaN thin films. The research in this paper helps us to better understand the growth processes and controllable growth of GaN thin films on a LT GaN/InGaN compliant substrate in a MOCVD system.

Acknowledgements

This work was supported by National Science Foundation of China (60776015 and 60976008), the Special Funds for Major State Basic Research Project (973 program) of China (2006CB604907) and the 863 High Technology R&D Program of China (2007AA03Z402 and 2007AA03Z451). We appreciate Prof. Huanhua Wang (Beijing Synchrotron Radiation Facility, Institute of High Energy Physics, Chinese Academy of Sciences) for his help in HRXRD measurements. We also acknowledge Prof. Yongliang Li (Analytical and Testing Center, Beijing Normal University) for FE-SEM measurements and Yang Li (University of Science and Technology Beijing) for useful discussions.

References

1 Lianshan Wang, Xianglin Liu, Yude Zan, Jun Wang, Du Wang, Dacheng Lu and Zhanguo Wang, *Appl. Phys. Lett.*, 1998, **72**, 109.
2 H. Marchand, X. H. Wu, J. P. Ibbetson, P. T. Fini, P. Kozodoy, S. Keller, J. S. Speck, S. P. DenBaars and U. K. Mishra, *Appl. Phys. Lett.*, 1998, **73**, 747.
3 J. Q. Liu, J. F. Wang, Y. X. Qiu, X. Guo, K. Huang, Y. M. Zhang, X. J. Hu, Y. Xu, K. Xu, X. H. Huang and H. Yang, *Semicond. Sci. Technol.*, 2009, **24**, 125007.
4 S. D. Lester, F. A. Ponce, M. G. Craford and D. A. Steigerwald, *Appl. Phys. Lett.*, 1995, **66**, 1249.
5 W. Qian, M. Skowronski, M. DeGraef, K. Doverspike, L. B. Rowland and D. K. Gaskill, *Appl. Phys. Lett.*, 1995, **66**, 1252.
6 X. H. Wu, L. M. Brown, D. Kapolnek, S. Keller, B. Keller, S. P. DenBaars and J. S. Speck, *J. Appl. Phys.*, 1996, **80**, 3228.
7 J. Cao, D. Pavlidis, A. Eisenbach, A. Philippe, C. Bru-Chevallier and G. Guillot, *Appl. Phys. Lett.*, 1997, **71**, 3880.
8 Z. C. Zhang, Y. H. Chen, D. B. Li, F. Q. Zhang, S. Y. Yang, B. S. Ma, G. S. Sun, Z. G. Wang and X. P. Zhang, *J. Cryst. Growth*, 2003, **257**, 321–325.
9 Hyun-Jae Lee, S. W. Lee, H. Goto, Sang-Hyun Lee, Hyo-Jong Lee, J. S. Ha, Takenari Goto, M. W. Cho and T. Yao, *Appl. Phys. Lett.*, 2007, **91**, 192108.
10 Anwar Hushur, Murli H. Manghnani and Jagdish Narayan, *J. Appl. Phys.*, 2009, **106**, 054317.
11 S. Tripathy, S. J. Chua, P. Chen and Z. L. Miao, *J. Appl. Phys.*, 2002, **92**, 3503.
12 Zhenjia Xu, *Diagnostical and Analytical Technology of Semiconductors Devices (in Chinese), Science*, Beijing, 2007, p. 143–144.
13 T. Detchprohm, K. Hiramatsu, K. Itoh and I. Akasaki, *Jpn. J. Appl. Phys.*, 1992, **31**, L1454–L1456.
14 Hock M. Ng, Nils G. Weimann and Aref Chowdhury, *J. Appl. Phys.*, 2003, **94**, 650.
15 Song-Bek Che, Wataru Terashima, Yoshihiro Ishitani, Akihiko Yoshikawa, Takeyoshi Matsuda, Hirotatsu Ishii and Seikoh Yoshida, *Appl. Phys. Lett.*, 2005, **86**, 261903.
16 O. H. Roh, Y. Tomita, M. Ohsugi, X. Wang, Y. Ishitani and A. Yoshikawa, *Phys. Status Solidi B*, 2004, **241**, 2835–2838.
17 O. Ambacher, M. S. Brandt, R. Dimitrov, T. Metzger, M. Stutzmann, R. A. Fischer, A. Miehr, A. Bergmaier and G. Dollinger, *J. Vac. Sci. Technol., B*, 1996, **14**, 3532.
18 Yoshinao Kumagai, Jun Kikuchi, Yuriko Matsuo, Yoshihiro Kangawa, Ken Tanaka and Akinori Koukitu, *J. Cryst. Growth*, 2004, **272**, 341.
19 Derrick S. Kamber, Yuan Wu, Edward Letts, Steven P. DenBaars, James S. Speck, Shuji Nakamura and Scott A. Newman, *Appl. Phys. Lett.*, 2007, **90**, 122116.

This journal is © The Royal Society of Chemistry 2010